International Journal of Environmental Sciences
ISSN: 2229-7359
Vol. 11 No. 2s, 2025
https://www.theaspd.com/ijes.php

Determine Potential Temperature, Hydrostatic Stability, and Thunderstorms Using CAPE, Case Study over Baghdad City

Ahmed A. Hashim[1], Salam K. Muhammed[1], Osama T. Al-Taai[1*], Fadwa S. Abdalfatah[1] and Zainab M. Abbood[1]
Department of Atmospheric Sciences, College of Sciences, Mustansiriyah University, Baghdad, Iraq.
*Corresponding Author E-mail: osamaaltaai77@uomustansiriyah.edu.iq

Abstract: In meteorology, the planetary boundary layer (PBL), often called the atmospheric boundary layer (ABL), is the lowest layer of the atmosphere. Its behavior is dictated by its direct contact with a planetary surface. On Earth, it usually responds to variations in surface radiative forcing in less than an hour. Intense vertical mixing and rapid variations in physical parameters including flow velocity, temperature, and moisture are present in the lowest layer. The wind is affected by surface drag and spins across the isobars in the open atmosphere above the PBL, where it normally flows parallel to the isobars. The European Centre for Medium-Range Weather Forecasts (ECMWF) collected data on temperature, dew point, atmospheric pressure, and height from satellites for height (32-26509.7) m, pressure levels (1000-20) mbar, and the selection of characteristic days of the month of 2018 for the Baghdad station to obtain the greatest number and variety of clouds and their use in the calculation of cloud cover and weather stability in terms of calculation daily change. To define the type of air stability, the potential temperature (ɵ) was also computed with height. Atmospheric stability was also estimated with the height of the cloud base and below the cloud base. The findings demonstrated that throughout the seasons, the atmosphere is either stable (St), unstable (UnSt), or neutral (Neu).
Keywords: PBL, CPB, CP, SBL, Iraq.

1. INTRODUCTION

In a convective planetary boundary layer, thermal instability brought on by positive buoyancy flux at the surface leads to additional or even significant turbulence [1][2]. Tropical and mid-latitude regions frequently see a convective boundary layer during the day [3][4][5]. The Free convective layer may cover the full troposphere up to the tropopause, which is situated between 10 and 18 kilometers above sea level in the Intertropical convergence zone, as a result of a combination of solar thermal and the heat break free during H_2O condensation [6][7][8]. The lower troposphere (CPBL), often referred to as the midday PBL (or simply the CBL), is the region most directly impacted by the sun's warmth on the earth's surface [9][10]. From the earth's surface to a capping inversion, this layer exists. which typically develops over land by midafternoon at a height of 1-2 km [11]. Inversion below the capping, also known as the entrainments zone during the daylight, which is 10–60% of CBL depth), The CBL is separated into two sub-layers: the surface layer (5–10%) and the mixed layer (35–80% of the CBL depth) [12][13]. Strong buoyancy formed by convective turbulent mixing causes the mixed layer, which makes most CBLs appear to have a highly consistent distribution of factors, such as potential temperatures, speed, moisture, and pollutant concentration [14][15]. The CBL's mixed layer turbulence frequently exhibits recognizable patterns like thermals and plumes [16], suggesting that it is not wholly random in comparison to simulations of smaller eddies created by local shearing in the surface layer; these massive eddies are very different [17][18]. The variables should take into account the massive eddies' non-local characteristics [19][20].

1.1. Stably stratified planetary boundary layer (SBL)

An SBL cannot exist without open atmospheric airflow and is only propelled by wind shear turbulence [21][22]. The SBL becomes a PBL when a negative buoyancy flux at the surface reduces the turbulence (see Convective inhibition) [23][24]. Anytime the Earth's surface is cooler than the atmosphere above, an SBL happens often at night [25][26]. In certain places, it might also happen throughout the day. In high latitudes, where it is typically persistent (days to months), an SBL is very significant and causes unusually cold air temperatures [27][28]. Physical principles and equations of motion, which are significantly non-linear and heavily impacted by Earth's features and the evolution of processes in the free atmosphere, control the

dynamics and microphysics of the PBL [29][29]. To tackle this complexity, the entire range of turbulence modeling has been proposed. Nevertheless, they often fail to meet practical requirements [30][31] The application of a large eddy simulations technique to PBL-related problems is anticipated to result in improvements [32][33][34]. The most important processes, the turbulent movements of contaminants (air pollutants) and moisture (evapotranspiration), depend critically on correct PBL modeling in atmospheric models [35][36]. Clouds in the boundary layer have an impact on the trade winds [37][38][39]. The three CBL layers' average characteristics are as follows [40][41][42]:

- The surfaces are a very thin area close to the ground that makes up the bottom 5% to 10% of the CBL. Severe wind shear, a super adiabatic lapse rate, and a decrease in moisture with height are its defining characteristics. The surface layer contains almost all of the wind shear and possible temperature gradients in the CBL.
- The Mixed layer, which makes up the middle 35% to 80% of CBL, conserves variables such as meteorological variables.
  The capping inversion, also known as the entrainment zone, can be rather thick, typically accounting for 40% of the CBL's depth. Entrainments of free atmosphere air downstream and overshooting thermals upwards occur in this area of static stable air towards the tops of the mixed layer [43][44]. The ɵ and speed increase dramatically while moisture drops across the capping inversion [45][46].

1.2. Literature review

The effects of thunderstorm prediction based on atmospheric stability and instability and reaching a dynamic equilibrium state have been the subject of numerous studies [47][48]:
and the outcome The association between CAPE and Cp and CAPE and Tp is positive at all sites; however, the correlation is very strong at the Mosul station and low at the Zakho station. Condensation, the airlifting mechanism, local geography, and weather conditions are the causes of this [14][49]. The lack of rainfall in Iraq is restricted to winter and the early spring and fall to a lesser extent, even though spring and autumn are less rainy because the Mediterranean declines are lessening their impact on the country and the area is being influenced by tropical continental air, which is characterized by drought. This is because medium atmospheric depressions are occurring more frequently. Therefore, excessive sun radiation, especially during the summer, leads to high evaporation and rising dryness [15][50]. The relationship between PBL and land surface and near-surface features that aren't specifically taken into account by conservation strategies was investigated using statistics. The results show that atmospheric stability in the layer of PBL expansion is the most significant element influencing PBL development. Furthermore, this study demonstrated high correlations between PBL height and soil moisture, potential temperature, and specific humidity; these parameters are considered the most important regulators of PBL growth [16][51]. Strong capping inversion and boundary layer stability cause dominating gravity waves to emerge at the top of the stable boundary layer. These waves seem to be connected to the most unstable wave predicted by the Taylor-Goldstein equation, as was studied. The jet's time-dependent behavior is compared using inertial oscillation analysis [17][52][53].

MATERIALS AND METHODS

1.3. Data and study region

The (ECMWF) collected data from satellites on temperature, dew point, atmospheric pressure, and height for height (32-26509.7) m, pressure levels (1000-20 mbar), and the choice of the characteristic days of the month of 2018 for the Baghdad station to obtain the greatest number and variety of clouds, which determined the atmospheric stability [54][55].

1.4. Potential temperature (ɵ)

The potential temperature of a fluid parcel at pressure P is the temperature. that a fluid parcel might achieve if adiabatically raised to a common standard pressure P, commonly 1000 hPa (1000 mbar). The ɵ is defined and determined as follows for an almost ideal gas [56][57]:

$$ɵ = T(\frac{P_s}{P})\text{^}0.286 \quad (1)$$

Where Cp is the specific heat capacity, R is the air gas constant, and T is the parcel's current absolute temperature (measured in K). For air (meteorology), R/Cp=0.286 [18][58].

Dynamically, ɵ is more significant than actual temperatures. This is because it is unaffected by the actual rising or sinking brought on by passing through barriers or violent air currents [59]. A parcel of air flowing over a miniature mountain will expand and warm as it ascends on one side and condense and warm as it lowers on the other in the absence of thermal, cold, evaporations, or condensations [60]. Because parcels with the same can interact without the requirement for labor or heating, lines with constant potential temperature are natural flow channels [19][61]. While the actual temperature may climb or fall, the increases in the atmosphere almost invariably [62]. In the PBL, which is frequently on the verge of becoming dry adiabatic, it is essential since it is conserved for all dry adiabatic operations [20][63]. The static stability of the UN-St. environments is well represented by the. Under normal, steadily stratified situations, vertical vibrations are attenuated and increase with height [64]. Convection is likely if the environment is UN-St. to vertical movements and the potential temperatures drop with height [21][65]. Except when significant convection is taking place or during times of severe insolation, reports of lowering with height are uncommon since convections act to swiftly mix the atmosphere and restore it to a stable stratified condition [22]. When the corresponding falls with height, indicating instability in saturated air, it occurs more frequently [23][66]. in steady, adiabatic flow because ɵ is preserved under adiabatic or isentropic air eddies. The isentropic analysis, a synoptic analytic method that enables the portrayal of air motions, particularly the study of large-scale vertical motion, uses these data [24] [67].

$$\begin{cases} \frac{\delta \theta}{\delta z} > 0 \text{ Stable} \\ \frac{\delta \theta}{\delta z} < 0 \text{ UN stable} \\ \frac{\delta \theta}{\delta z} = 0 \text{ Neutral} \end{cases} \quad (2)$$

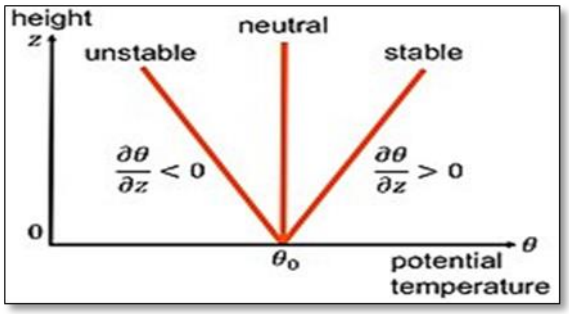

Figure 1. Explain Potential temperature and hydrostatic stability [26].

2. RESULTS AND DISCUSSION

2.1. The behaviors of thunderstorms for the winter season in Baghdad

Figure 2, show that 1 Dec 2018 (00:00 am) was medium clouds at a pressure level between (125 and 650 mbar) this type from clouds was nimbostratus whereas 1 Dec 2018 (12:00 pm) was high clouds at pressure level between (150 and 400 mbar) this type from clouds was not include thunderstorms. 1 Jan 2018 (00:00 am) was medium clouds at pressure level between (150 and 700 mbar) this type from clouds was nimbostratus whereas 1 Jan 2018 (12:00 pm) was high clouds at pressure level between (150 and 300 mbar) this type from clouds was not include thunderstorms where weather was clear. 16 Feb 2018 (00:00 am) was low clouds at pressure level between (175 and 850 mbar) this type from clouds was cumulonimbus that represent major source for thunderstorms also high potential temperature whereas 1 Feb 2018 (12:00 pm) was high clouds at a pressure level between (200 and 400 mbar) this type from clouds was medium clouds (Altostratus) that not include thunderstorm. High clouds represent a stable atmosphere, medium clouds represent an unstable atmosphere, and low clouds represent an unstable atmosphere at that time. This is caused by astronomical and meteorological causes, climate variations, and surface characteristics. Heavy thunderstorms are present on the

days when there is the most rain. Additionally, thunderstorms are the primary source of convective energy in the clouds. Thunderstorm damage is primarily brought on by strong winds, hail, and flooding.

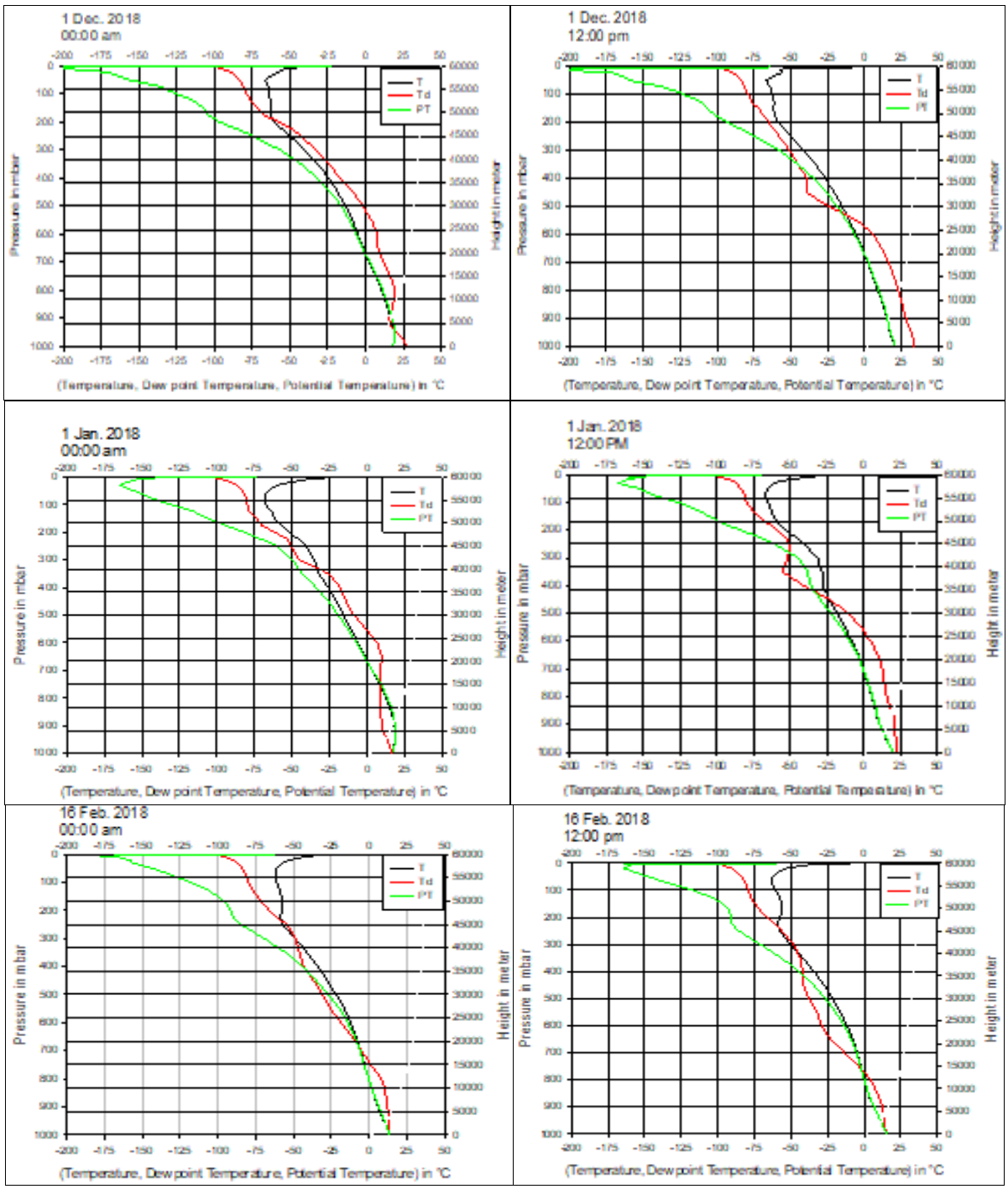

Figure 2. Determine temperature, dew point temperature, and potential temperature by using (T- ϕ -gram) over Baghdad city at hours (mid-day and mid-night) for the days (01 Dec., 01 Jan., and 16 Feb.) of the year 2018.

2.2. The analysis of thunderstorms for the spring season in Baghdad

Figure 3 shows that on 1 Mar 2018 (00:00 am), there were high clouds at pressure levels between 300 and 450 mbar. whereas 1 Mar 2018 (12:00 pm) was high clouds at pressure level between (225 and 600 mbar) this type from clouds was not include thunderstorms. 1 April 2018 (00:00 am) was low clouds at pressure level between

(200 and 1000 mbar) this type from clouds was cumulonimbus that represent major source for thunderstorms also high potential temperature whereas 1 May 2018 (12:00 pm) was high clouds at pressure level between (175 and 1000 mbar) this type from clouds was low clouds (Cb). 1 May 2018 (00:00 am) was high clouds at a pressure level between (200 and 400 mbar) whereas 1 Apr 2018 (12:00 pm) was high clouds at a pressure level between (200 and 400 mbar) this type of clouds was not include thunderstorms where weather was clear. High clouds represent a stable atmosphere, medium clouds represent an unstable atmosphere, and low clouds represent an unstable atmosphere at that time. This is caused by astronomical and meteorological causes, climate variations, and surface characteristics. Heavy thunderstorms are present on the days when there is the most rain. Additionally, thunderstorms are the primary source of convective energy in the clouds. Thunderstorm damage is primarily brought on by strong winds, hail, and flooding.

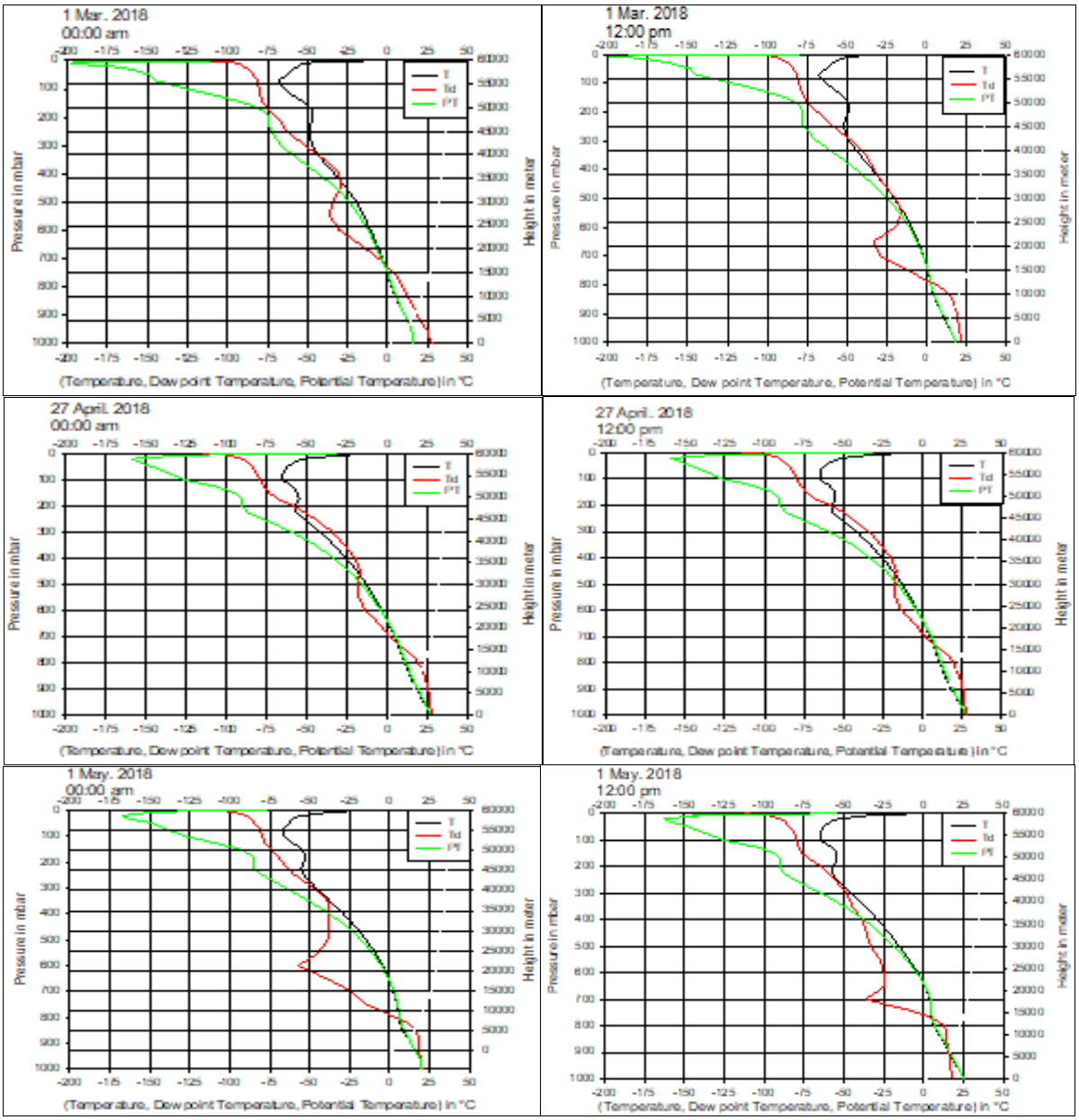

Figure 3. Determine temperature, dew point temperature, and potential temperature by using (T- ϕ -gram) over Baghdad city at hours (mid-day and mid-night) for the days (01 Mar., 27 Apr., and 01 May) of the year 2018.

2.3. The analysis of thunderstorms for the summer season in Baghdad

The Fig. 4, show that 2 June 2018 (00:00 am) was low clouds at pressure level between (500 and 1000 mbar) this type from clouds was cumulus whereas 2 June 2018 (12:00 pm) was high clouds at pressure level between (775 and 1000 mbar) this type from clouds was not include thunderstorms. 1 July 2018 (00:00 am) was medium clouds at pressure level between (150 and 700 mbar) this type from clouds was nimbostratus whereas 1 July 2018 (12:00 pm) was high clouds at pressure level between (150 and 300 mbar) this type from clouds was not include thunderstorms where weather was clear. 1 Aug 2018 (00:00 am) was low clouds at a pressure level between (925 and 950 mbar) this type of clouds was stratus whereas 1 Aug 2018 (12:00 pm) was high clouds at a pressure level between (825 and 875 mbar) this type from clouds was low clouds that not include thunderstorm. High clouds represent a stable atmosphere, medium clouds represent an unstable atmosphere also low clouds represent an unstable atmosphere at that time. this is caused by astronomical and meteorological causes, climate variations, and surface characteristics. Heavy thunderstorms are present on the days when there is the most rain. Additionally, thunderstorms are the primary source of convective energy in the clouds. Thunderstorm damage is primarily brought on by strong winds, hail, and flooding.

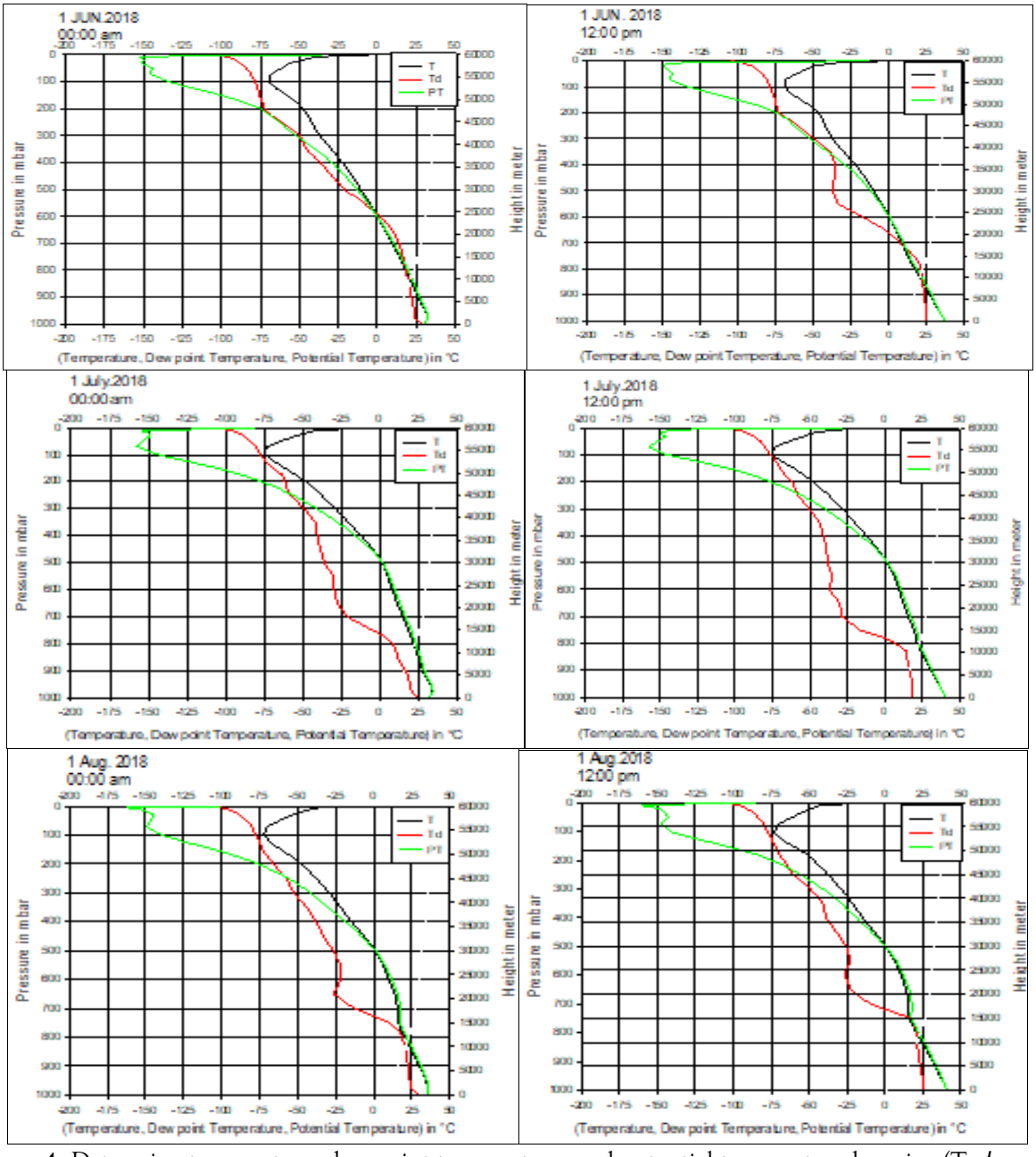

Figure 4. Determine temperature, dew point temperature, and potential temperature by using (T- ϕ -gram) over Baghdad city at hours (mid-day and mid-night) for the days (Jun., 01 Jul., and 01 Aug.) of the year 2018.

International Journal of Environmental Sciences
ISSN: 2229-7359
Vol. 11 No. 2s, 2025
https://www.theaspd.com/ijes.php

2.4. The analysis of thunderstorms for the autumn season in Baghdad

Fig. 5 shows that on 1 Sep 2018 (00:00 am), there were high clouds at pressure levels between 70 and 250 mbar. This type of cloud was cirrus, whereas on 1 Sep. 2018 (12:00 pm), there were high clouds at pressure levels between 70 and 250 mbar. This type of clouds does not include thunderstorms. 26 Oct 2018 (00:00 am) was low clouds at pressure level between (100 and 1000 mbar) this type from clouds was Cb whereas 1 Oct. 2018 (12:00 pm) was low clouds at pressure level between (100 and 1000 mbar). 1 Nov 2018 (00:00 am) was high clouds at pressure levels between (125 and 600 mbar), whereas 1 Nov. 2018 (12:00 pm) was high clouds at a pressure level between (125 and 600 mb). This type of clouds was high clouds that did not include thunderstorms. High clouds represent a stable atmosphere, medium clouds represent an unstable atmosphere, and low clouds represent an unstable atmosphere at that time. This is caused by astronomical and meteorological causes, climate variations, and surface characteristics. Heavy thunderstorms are present on the days when there is the most rain. Additionally, thunderstorms are the primary source of convective energy in the clouds. Thunderstorm damage is primarily brought on by strong winds, hail, and flooding.

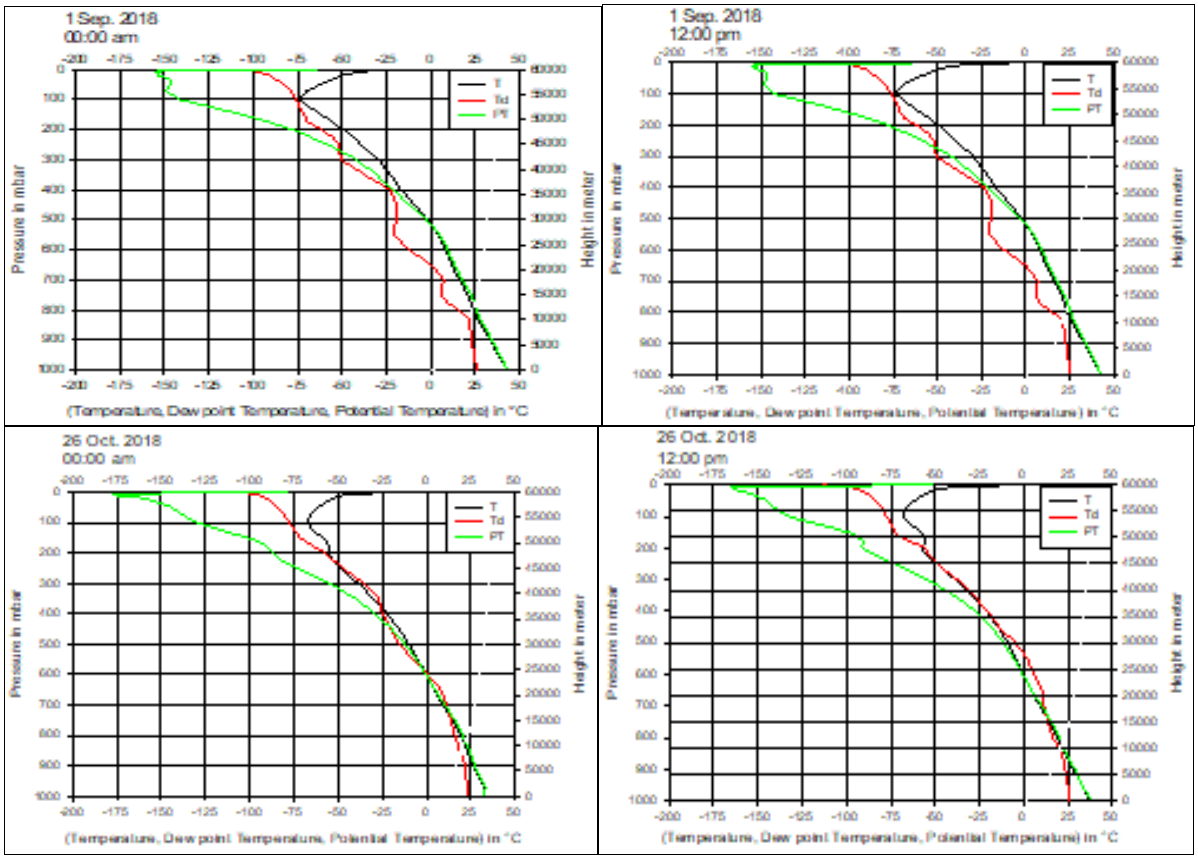

International Journal of Environmental Sciences
ISSN: 2229-7359
Vol. 11 No. 2s, 2025
https://www.theaspd.com/ijes.php

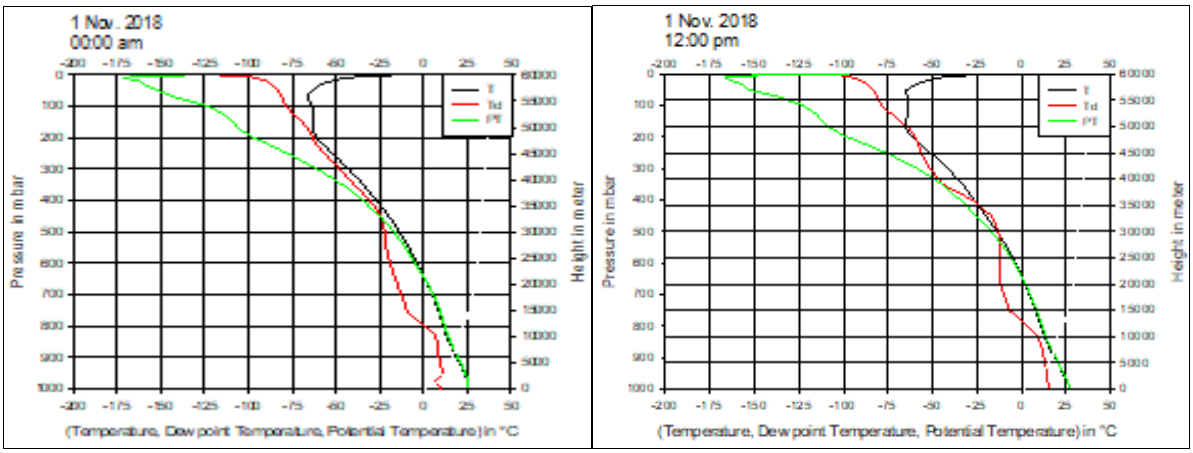

Figure 5. Determine temperature, dew point temperature, and potential temperature by using (T- ϕ -gram) over Baghdad city at hours (mid-day and mid-night) for the days (01 Sep., 26 Oct., and 01 Nov.) of the year 2018.

2.5. Forecasting thunderstorms using CAPE for four seasons over Iraq

A thunderstorm can only form if three conditions are met: moisture, ascending unstable air, and rising air. A lifting device that continues to raise even after being nudged is used to deliver the nudge. The sun warms the Earth's surface, warming the air above it as well. Thunder is the acoustic effect that a thunderstorm—also called an electrical storm or a lightning storm—has on the atmosphere of the Earth. "Thundershowers" are short-lived thunderstorms. One kind of cloud where thunderstorms form is a cumulonimbus. Often they bring torrential rain, snow, sleet, or hail, and they are often accompanied by strong gusts. Some thunderstorms, nevertheless, produce little to no precipitation. Thunderstorms are caused by hot, humid air that rises quickly. Warm, humid air rises, cools, condenses, and then rises again to form cumulonimbus clouds. These clouds have a 20-kilometer altitude range. As the rising air reaches its dew point temperature, water vapor condenses into water droplets or ice, reducing local pressure inside the thunderstorm cell. Before it reaches the earth, any precipitation must travel a considerable distance through the clouds. The droplets get bigger as they descend and hit with each other. A downdraft is created when raindrops fall because they bring chilly air with them. As it spreads in the direction of the Earth's surface, this cold air occasionally creates strong winds that are frequently linked to thunderstorms. Thunderstorms can form and develop anywhere in the world, but they seem to do so most frequently in the mid-latitudes, where warm, moist air from tropical latitudes meets chilly air from polar latitudes. Numerous severe weather events originate and occur as a result of thunderstorms. Thunderstorms and the associated phenomena provide serious risks. Large hailstones, downburst winds, and flash flooding brought on by intense precipitation are the main causes of damage from thunderstorms. As shown in Figures 6–8, stronger thunderstorm cells have the potential to produce tornadoes and waterspouts.

International Journal of Environmental Sciences
ISSN: 2229-7359
Vol. 11 No. 2s, 2025
https://www.theaspd.com/ijes.php

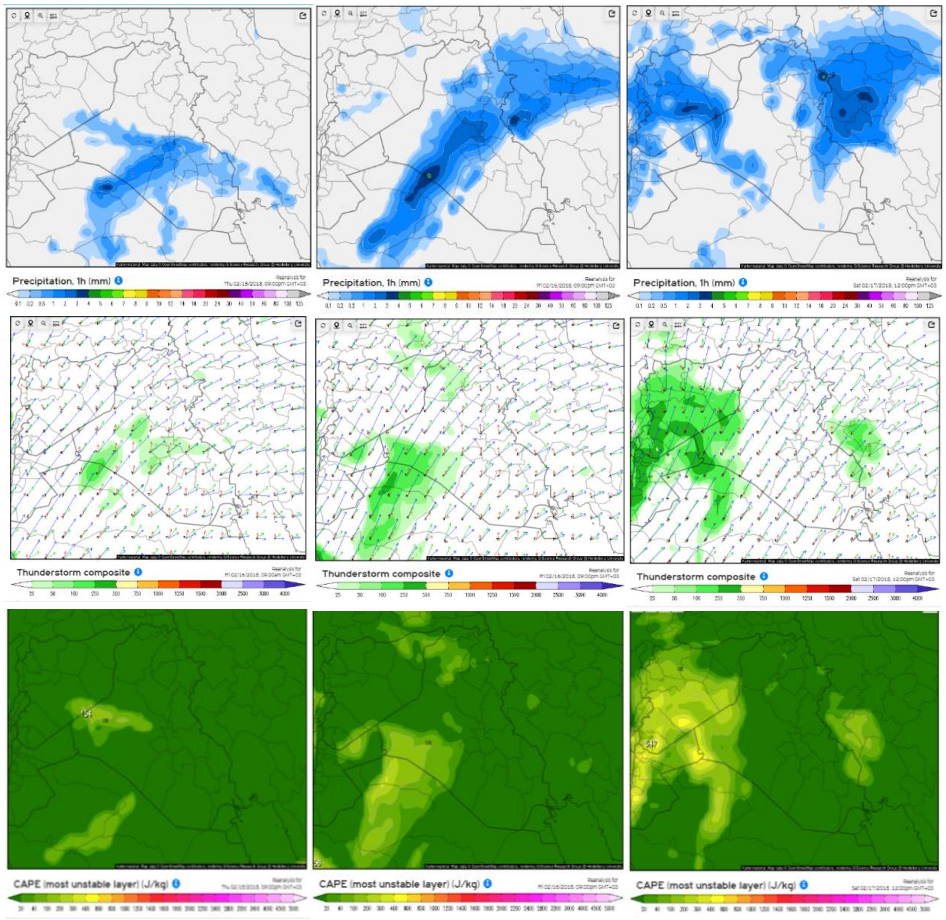

Figure 6. For the Baghdad station, the most precipitation fell on February 16, 2018, at 9:00 p.m., but the thunderstorm (CAPE) appeared to form on February 15, developed on February 16, and then started to dissipate on February 17.

International Journal of Environmental Sciences
ISSN: 2229-7359
Vol. 11 No. 2s, 2025
https://www.theaspd.com/ijes.php

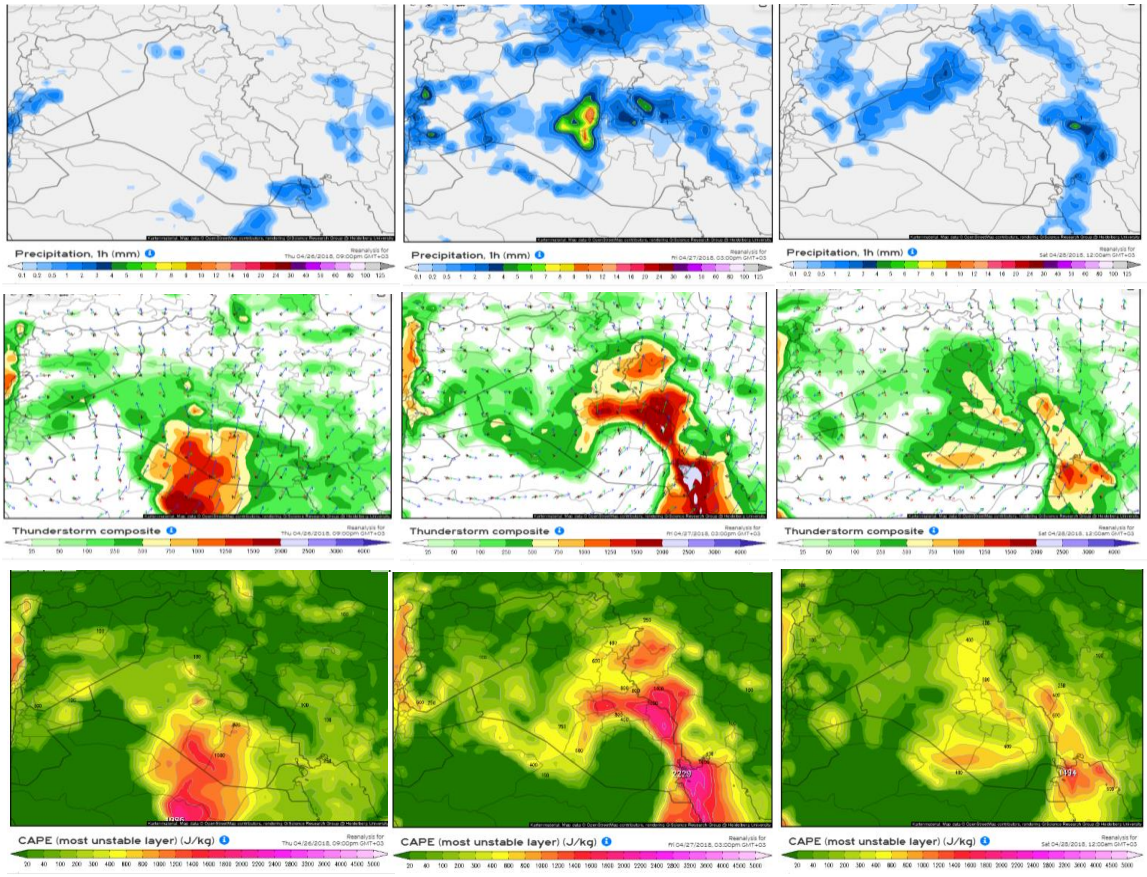

Figure 7. for the Baghdad station the thunderstorm (CAPE) appeared to begin on day 26/04/2018, developed on day 27/04/2018, and then started to disperse on day 28/04/2018, the maximum amount of total precipitation fell on day 27/04/2018 (03:00 pm).

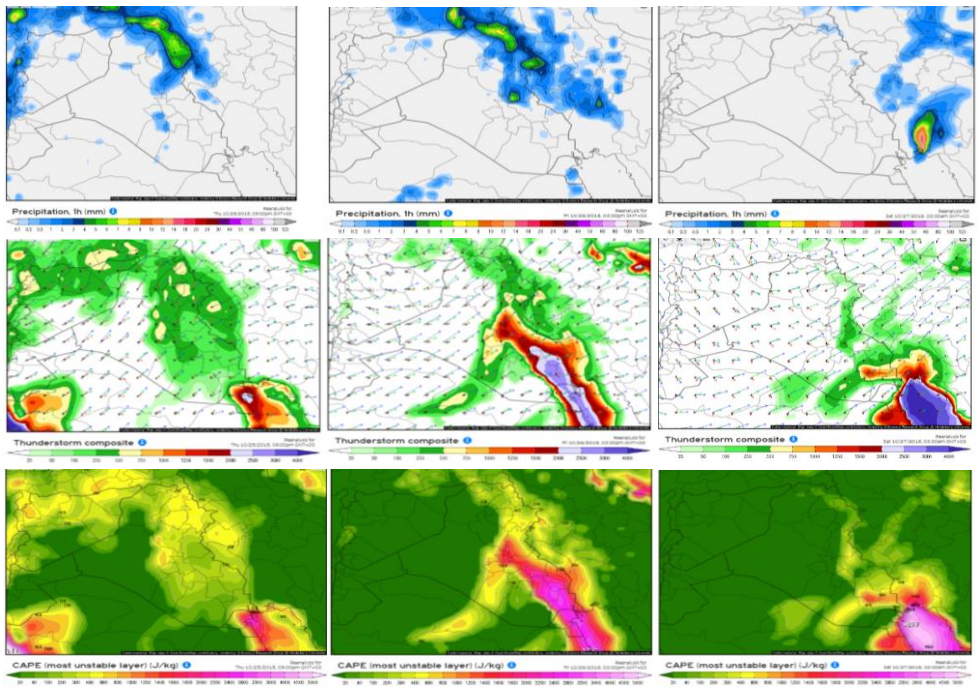

Figure 8. For the Baghdad station, the most precipitation fell on October 26, 2018, at 3:00 p.m., but the thunderstorm (CAPE) first appeared to form on October 25, developed on October 26, and then started to disperse on October 27.

CONCLUSIONS

For the winter season, the day with the most total precipitation was February 16, 2018. On April 27, 2018, there was the most precipitation overall for the spring season. On October 26, 2018, there was the most precipitation overall during the autumn season. Heavy thunderstorms are present on the days when there is the most rain. Additionally, thunderstorms are the primary source of convective energy in the clouds. Thunderstorm damage is primarily brought on by strong winds, hail, and flooding. Due to meteorological and astronomical causes, climatic fluctuations, and the makeup of the surface, low clouds at that moment reflect an unstable atmosphere, whereas medium and high clouds represent stable atmospheres. the possible temperature, too. While the thunderstorm (CAPE) appeared to begin on day 26/04/2018, developed on day 27/04/2018, and then started to disperse on day 28/04/2018, the maximum amount of total precipitation fell for the Baghdad station on day 27/04/2018 (03:00 pm).

Acknowledgment

An acknowledgment to the European Centre Medium Weather Forecasts (ECMWF) and acknowledgment to Mustansiriyah University.

REFERENCES

1. Hu, X.-M., J.W. Nielsen-Gammon, and F. Zhang, Evaluation of three planetary boundary layer schemes in the WRF model. Journal of Applied Meteorology and Climatology, 2010. 49(9): p. 1831-1844.
2. Buske, D., et al., Simulation of pollutant dispersion for low wind conditions in stable and convective planetary boundary layer. Atmospheric Environment, 2007. 41(26): p. 5496-5501.
3. Flamant, C., et al., Airborne observations of the impact of a convective system on the planetary boundary layer thermodynamics and aerosol distribution in the inter-tropical discontinuity region of the West African monsoon. Quarterly Journal of the Royal Meteorological Society: A journal of the atmospheric sciences, applied meteorology and physical oceanography, 2007. 133(626): p. 1175-1189.
4. Wisse, J. and J. Vilà-Guerau de Arellano. Analysis of the role of the planetary boundary layer schemes during a severe convective storm. in Annales Geophysicae. 2004. Copernicus GmbH.
5. Coniglio, M.C., et al., Verification of convection-allowing WRF model forecasts of the planetary boundary layer using sounding observations. Weather and Forecasting, 2013. 28(3): p. 842-862.
6. Patton, E.G., P.P. Sullivan, and C.-H. Moeng, The influence of idealized heterogeneity on wet and dry planetary boundary layers coupled to the land surface. Journal of Atmospheric Sciences, 2005. 62(7): p. 2078-2097.
7. Temel, O., et al., Large eddy simulations of the Martian convective boundary layer: towards developing a new planetary boundary layer scheme. Atmospheric Research, 2021. 250: p. 105381.
8. Spiga, A., et al., A study of daytime convective vortices and turbulence in the martian Planetary Boundary Layer based on half-a-year of InSight atmospheric measurements and Large-Eddy Simulations. Journal of Geophysical Research: Planets, 2021. 126(1): p. e2020JE006511.
9. Cintineo, R., et al., Evaluating the performance of planetary boundary layer and cloud microphysical parameterization schemes in convection-permitting ensemble forecasts using synthetic GOES-13 satellite observations. Monthly Weather Review, 2014. 142(1): p. 163-182.
10. Zhou, B., Y. Li, and K. Zhu, Improved length scales for turbulence kinetic energy–based planetary boundary layer scheme for the convective atmospheric boundary layer. Journal of Atmospheric Sciences, 2020. 77(7): p. 2605-2626.
11. Flaounas, E., S. Bastin, and S. Janicot, Regional climate modeling of the 2006 West African monsoon: sensitivity to convection and planetary boundary layer parameterization using WRF. Climate Dynamics, 2011. 36(5): p. 1083-1105.
12. Schwitalla, T., O. Branch, and V. Wulfmeyer, a Sensitivity study of the planetary boundary layer and microphysical schemes to the initialization of convection over the Arabian Peninsula. Quarterly Journal of the Royal Meteorological Society, 2020. 146(727): p. 846-869.

13. Bogenschutz, P., et al., Unified parameterization of the planetary boundary layer and shallow convection with a higher-order turbulence closure in the Community Atmosphere Model: Single-column experiments. Geoscientific Model Development, 2012. 5(6): p. 1407-1423.
14. Al-Taai, O.T. and Z.M. Abbood, Analysis of the convective available potential energy by precipitation over Iraq using ECMWF data for the period of 1989–2018. Przegląd Naukowy Inżynieria i Kształtowanie Środowiska, 2020. 29.
15. Al-Taai, O.T. and Z.M. Abbood, Analysis of convective available potential energy by convective and total precipitation over Iraq. Indian Journal of Ecology, 2020. 47(10): p. 263-269.
16. Santanello Jr, J.A., M.A. Friedl, and W.P. Kustas, An empirical investigation of convective planetary boundary layer evolution and its relationship with the land surface. Journal of Applied Meteorology, 2005. 44(6): p. 917-932.
17. Saiki, E.M., C.-H. Moeng, and P.P. Sullivan, Large-eddy simulation of the stably stratified planetary boundary layer. Boundary-Layer Meteorology, 2000. 95(1): p. 1-30.
18. Jackett, D.R., et al., Algorithms for density, potential temperature, conservative temperature, and the freezing temperature of seawater. Journal of Atmospheric and Oceanic Technology, 2006. 23(12): p. 1709-1728.
19. Wang, X., et al., Finite element modelling of electric current-activated sintering: The effect of coupled electrical potential, temperature and stress. Acta Materialia, 2007. 55(10): p. 3611-3622.
20. Varga, R., et al., OTOF mutations revealed by genetic analysis of hearing loss families including a potential temperature sensitive auditory neuropathy allele. Journal of medical genetics, 2006. 43(7): p. 576-581.
21. Tremblin, P., et al., Advection of potential temperature in the atmosphere of irradiated exoplanets: a robust mechanism to explain radius inflation. The Astrophysical Journal, 2017. 841(1): p. 30.
22. Green, D.H. and T.J. Falloon, Primary magmas at mid-ocean ridges," hotspots," and other intraplate settings: Constraints on mantle potential temperature. Special Papers-Geological Society of America, 2005. 388: p. 217.
23. Revil, A., et al., Inner structure of La Fossa di Vulcano (Vulcano Island, southern Tyrrhenian Sea, Italy) revealed by high-resolution electric resistivity tomography coupled with self-potential, temperature, and CO_2 diffuse degassing measurements. Journal of Geophysical Research: Solid Earth, 2008. 113(B7).
24. Zhou, B., Y. Li, and K. Zhu, Improved length scales for turbulence kinetic energy–based planetary boundary layer scheme for the convective atmospheric boundary layer. Journal of Atmospheric Sciences, 2020. 77(7): p. 2605-2626.
25. Lothon, M., D.H. Lenschow, and S.D. Mayor, Doppler lidar measurements of vertical velocity spectra in the convective planetary boundary layer. Boundary-layer meteorology, 2009. 132(2): p. 205-226.
26. Hu, X.-M., J.W. Nielsen-Gammon, and F. Zhang, Evaluation of three planetary boundary layer schemes in the WRF model. Journal of Applied Meteorology and Climatology, 2010. 49(9): p. 1831-1844.
27. W. G. Nassif, O. T. Al-Taai, and I. H. Abdalkareem, "Analysis of the Aerosol Optical Thickness and Winds Over Selected Stations in Iraq," AIP Conference Proceedings, 2021; 2372, p. 030008.
28. O. F. Khayoon, and O. T. Al-Taai, "Severe Meteorological Factors Affecting Civil Aviation Flights at Iraqi Airports," Al-Mustansiriyah Journal of Science, vol. 33, no. 4, pp. 15-26, 2022.
29. Z. M. MohammedSalih, and O. T. Al-Taai, "The Effect of Temperature and Relative Humidity on Concentrations of Suspended Particles Matter (PM10, TSP) Recorded in Al-Waziriyah Station," Al-Mustansiriyah J. of Science, vol. 26, no. 2, pp. 65-73, 2015.
30. T. K. Jawad, and O. T. Al-Taai, "The Effect of Temperature on Soil Water Content in Baghdad City," Al-Mustansiriyah J. of Science, vol. 24, no. 6, pp. 95-104, 2013.
31. Z. M. Abbood, and O. T. Al-Taai, "Study of Absorbance and Emissivity Solar Radiation by Clouds, Aerosols and Some Atmospheric Gases," Journal of Applied and Advanced Research, vol. 3, no. 5, pp. 128-134, 2018.
32. W. G. Nassif, O. T. Al-Taai, and Z. M. Abbood, "The Influence of Solar Radiation on Ozone Column Weight Over Baghdad City," IOP Conference Series: Materials Science and Engineering, IOP Publishing, vol. 928, no. 7, p. 072089, 2020.

33. Z. M. Abbood, and O. T. Al-Taai, "Data Analysis for Cloud Cover and Rainfall over Baghdad City, Iraq," Plant Archives, vol. 20, no. 1, pp. 822-826, 2020.
34. Z. M. Abbood, and O. T. Al-Taai, "Calculation of Absorption and Emission of Thermal Radiation by Clouds Cover," ARPN Journal of Engineering and Applied Sciences, vol. 13, no. 24, pp. 9446-9456, 2018.
35. S. A. Hashim, W. G. Nassif, B. I. Wahab, Z. M. Abbood, O. T. Al-Taai, and Z. S. Mahdi, "Impact of COVID-19 on Aerosol Optical Depth and Particulate Matter over Iraq," Journal of Engineering Science and Technology, vol. 17, pp. 12-20, 2022.
36. O. T. Al-Taai, Z. M. Abbood, and J. H. Kadhum, "Determination Stability Potential Energy of Thunderstorms for Some Severe Weather Forecasting Cases in Baghdad City," Journal of Green Engineering, vol. 11, no. 1, pp. 779-794, 2021.
37. S. A. Hashim, J. H. Kadhum, Z. M. Abbood, O. T. Al-Taai, and W. G. Nassif, "Determination of the Dynamics of Thunderstorms Through the Dry Adiabatic Lapse Rate and Environmental Lapse Rate," Nature Environment and Pollution Technology, vol. 22, no. 3, pp. 1447-1455, 2023.
38. W. G. Nassif, F. H. Lagenean, and O. T. Al-Taai, "Impact of Vegetation Cover on Climate Change in Different Regions of Iraq," Caspian Journal of Environmental Sciences, vol. 21, no. 2, pp. 333-342, 2023.
39. R. S. Al-Awadi, O. T. Al-Taai, and S. A. Abdullah, "Assessment of Outer Space Events on Troposphere and Climate Change over Iraq," Iraqi Journal of Science, vol. 64, no. 8, pp. 4278-4289, 2023.
40. G. A. Redah, M. H. Al-Jiboori, and O. T. Al-Taai, "Turbulent Diffusion Effect on PM2.5 Concentration Above an Urban Canopy," IOP Conference Series: Earth and Environmental Science, IOP Publishing, vol. 1223, no. 1, p. 012005, 2023.
41. Z. M. Abbood, M. H. Al-Jiboori, and O. T. Al-Taai, "Temporal and Spatial Analysis of Particulate Matter Concentrations in Iraq," IOP Conference Series: Earth and Environmental Science, IOP Publishing, vol. 1215, no. 1, p. 012018, 2023.
42. O. T. Al-Taai, S. A. Hashim, W. G. Nassif, and Z. M. Abbood, "Interference between Total Solar Radiation and Cloud Cover over Baghdad City," Journal of Physics: Conference Series, vol. 2114, no. 1, p. 012070, 2021.
43. A. Al-Behadili, A. H. A. Al-Muhyi, and O. T. Al-Taai, "Analyzing the Oil Pollution Resulting from The Iraqi Oil Ports in The Northern Arabian Gulf Using the GNOME Model," AIP Conference Proceedings, AIP Publishing, vol. 2830, no. 1, p. 050004, 2023.
44. G. A. Redah, M. H. Al-Jiboori, and O. T. Al-Taai, "A Study of Turbulent Fluctuation of Three-Component Wind and Air Temperature in the Surface Layer of Baghdad Urban," IOP Conference Series: Earth and Environmental Science, IOP Publishing, vol. 1223, no. 1, p. 012005, 2023.
45. Z. M. Abbood, O. T. Al-Taai, and W. G. Nassif, "Impact of Wind Speed and Direction on Low Cloud Cover over Baghdad City," Current Applied Science and Technology, vol. 21, no. 3, pp. 590-600, 2021.
46. T. K. Jawad, O. T. Al-Taai, and Y. K. Al-Timimi, "Evaluation of drought in Iraq using DSI by remote sensing," Iraqi Journal of Agricultural Sciences, vol. 49, no. 6, pp. 1132-1145, 2018.
47. O. T. Al-Taai, "Preface," IOP Conference Series: Earth and Environmental Science, vol. 1223, no. 1, p. 011001, 2023.
48. W. G. Nassif, I. K. Al-Ataby, O. T. Al-Taai, and Z. M. Abbood, Impact of Soil Temperature and Precipitation on Vegetation Cover Over Selected Stations in Iraq, Asian Journal of Water, Environment and Pollution, 2024, 21(1), pp. 25–33.
49. W. G. Nassif, A. A. Hashim, S. A. Muter, and O. T. Al-Taai, Relationship Between Winds with Surface Roughness and Carbon Dioxide Concentrations Over Iraq, Asian Journal of Water, Environment and Pollution, 2024, 21(1), pp. 89–96.
50. R. M. Ibrahim, Z. M. Abbood, O. T. Al-Taai, and M. M. Ahmed, The Influence of Ozone Depletion Potential Weighted Anthropogenic Emissions of Nitrous Oxide, Asian Journal of Water, Environment and Pollution, 2024, 21(2), pp. 65–73.
51. W. G. Nassif, F. H. S. Lagenean, and O. T. Al-Taai, Impact of vegetation cover on climate change for different regions in Iraq, Journal of Agrometeorology, 2022, 24(2), pp. 138–145.
52. W. G. Nassif, F. H. Jasim, and O. T. Al-Taai, Analysis of air temperature, relative humidity and evaporation over Iraq using ECMWF reanalysis, Indian Journal of Ecology, 2021, 48(2), pp. 446–452.

53. S. J. Al-Jaf, and O. T. Al-Taai, Impact of carbon dioxide concentrations on atmospheric temperature changes over Iraq and some neighboring countries, Plant Archives, 2019, 19, pp. 1450–1456.
54. Z. M. Abbood, and O. T. Al-Taai, Data analysis for cloud cover and rainfall over Baghdad City, Iraq, Plant Archives, 2020, 20(1), pp. 822–826.
55. Z. M. Abbood, O. T. Al-Taai, and W. G. Nassif, Impact of wind speed and direction on low cloud cover over Baghdad city, Current Applied Science and Technology, 2021, 21(3), pp. 590–600.
56. Abd, N.M., Abbood, Z.M., Mohammed, N.A., Al-Taai, O.T., Nassif, W.G. Impact of Acid Gases on Total Precipitation Over Iraqi Stations. Nature Environment and Pollution Technology, 2025, 24, pp. 439–448.
57. Maan, H., Al-Taai, O.T., Halos, S.H. Estimate the drought in some Iraqi meteorological stations using the de Martonne Aridity index. AIP Conference Proceedings, 2024, 3229(1), 050014.
58. Nassif, W.G., Hashim, A.A., Muter, S.A., Al-Taai, O.T. Relationship Between Winds with Surface Roughness and Carbon Dioxide Concentrations Over Iraq. Asian Journal of Water, Environment and Pollution, 2024, 21(1), pp. 89–96.
59. Maan, H., Al-Taai, O.T., Halos, S.H. Calculating the Environmental Drought Index using the de Martonne Equation for the Rainy Months in Iraq. IOP Conference Series: Earth and Environmental Science, 2024, 1371(2), 022001.
60. Hashim, S.A., Tawfeek, Y.Q., Al-Taai, O.T., Abbood, Z.M. Spatiotemporal Distribution of the Monthly and Seasonal Mean of High Vegetation Cover, Total Precipitation, and Temperature in Iraq for the Period (1950-2022). IOP Conference Series: Earth and Environmental Science, 2024, 1371(2), 022008.
61. Ibrahim, R.M., Abbood, Z.M., Al-Taai, O.T., Ahmed, M.M. The Influence of Ozone Depletion Potential Weighted Anthropogenic Emissions of Nitrous Oxide. Asian Journal of Water, Environment and Pollution, 2024, 21(2), pp. 65–73.
62. Al-Amery, H.A., Al-Taai, O.T. The ozone effect on shortwave solar radiation in the atmosphere over Iraq. AIP Conference Proceedings, 2020, 2290, 0027825.
63. Nassif, W.G., Al-Taai, O.T., Muter, S.A. Inference of dynamically dust storms by relying on aerosolos optical thickness in Iraq. Journal of Green Engineering, 2021, 11(1), pp. 530–546.
64. Salman, A.D., Al-Taai, O.T. Association Between Precipitable Water Vapor and Evaporation Over Iraq During the Period (1979-2019). IOP Conference Series: Earth and Environmental Science, 2022, 1060(1), 012021.
65. Al-Awadi, R.S., Al-Taai, O.T., Abdullah, S.A. Assessment of X-Ray Effects on HF Radio Communications. IOP Conference Series: Earth and Environmental Science, 2023, 1223(1), 012003.
66. Al-Behadili, A.A., Al-Taai, O.T., Al-Muhyi, A.H.A. Analysis of ship accident resulting from bad weather conditions in the port of Khor Al-Zubair, Iraqi crane accident Aba Thar: a case study. Bionatura, 2023, 8(1), 49.
67. Al-Taai, O.T. Preface. IOP Conference Series: Earth and Environmental Science, 2023, 1223(1), 011001.